Electronic Supplementary Material (ESI) for Environmental Science: Nano.
This journal is © The Royal Society of Chemistry 2023

Supplementary Material

for

Efficient degradation of organic contaminants via a novel iron-based poly(ionic liquid)/polydopamine composite as the heterogeneous Fenton catalyst

Ruiqing Li [a], Yuyu Guo [a], Guifeng Ma [a], Daniel T. Sun [b, c], Ju Lin [a], Tianwei Xue [a], Rongxing Qiu [a], Sen Yan [a], Shuliang Yang [d], Yanliang Wang [a], Yanzhen Hong [a], Yuzhong Su [a], Hongtao Wang [a], Li Peng * [a], Jun Li * [a, e, f]

[a] College of Chemistry and Chemical Engineering, Xiamen University, Xiamen 361005, China

[b] Sunchem LLC, San Francisco, CA 94103, United States

[c] The Molecular Foundry, Lawrence Berkeley National Laboratory, 1 Cyclotron Road, Berkeley, California 94720, United States

[d] College of Energy, Xiamen University, Xiamen 361005, China

[e] National Engineering Laboratory for Green Chemical Productions of Alcohols, Ethers and Esters, Xiamen University, Xiamen 361005, China

[f] Collaborative Innovation Center of Chemistry for Energy Materials, Xiamen University, Xiamen 361005, China

* Corresponding Authors:

Tel: 86-0592-2185372. E-mail: li.peng@xmu.edu.cn (Li Peng); junnyxm@xmu.edu.cn (Jun Li).

List of captions:

Figure S1. ^{1}H NMR spectrum of the as-synthesized free base DA.
Figure S2. (a) SEM image, (b) EDS spectrum of PDVIm-Cl and (c) the corresponding elemental mappings of C, Cl and N.
Figure S3. (a) SEM image, (b) EDS spectrum of PDVIm-Fe and (c) the corresponding elemental mappings of C, Fe, S and N.
Table S1. The element content of PDVIm-Fe, PDVIm-Fe/PDA
Figure S4. (a) N_2 adsorption and desorption isotherms and (b) pore size distribution curve of PDVIm-Fe.
Figure S5. FT-IR spectra of PDVIm-Cl (grey), PDVIm-Fe (blue) and PDVIm-Fe/PDA (red).
Figure S6. Standard curve of the different concentrations of MG.
Figure S7. (a) Plots of relative concentration (C_t/C_0) changes of MG and (b) kinetic plots for the degradation of MG under different amounts of H_2O_2.
Figure S8. (a) Plots of relative concentration (C_t/C_0) changes of MG and (b) kinetic plots for the degradation of MG under different amounts of AA.
Figure S9. (a) Plots of relative concentration (C_t/C_0) changes of MG and (b) kinetic plots for the degradation of MG under different amounts of catalyst.
Table S2. The rate constants of MG degradation by PDVIm-Fe/PDA.
Figure S10. The influence of various quenchers on MG degradation by PDVIm-Fe/PDA.
Figure S11. The detected radical concentrations produced by PDVIm-Fe/PDA at different times.
Table S3. The TOC values in the MG degradation process catalyzed by PDVIm-Fe/PDA.
Figure S12. (a) The degradation efficiency of PDVIm-Fe and Fe/PDA on MG and (b) their recyclability.

Figure S13. (a) Fe leaching in the solution in each cycling test and (b) percent of Fe leaching in the solution compared with the original iron content in the catalyst.
Figure S14. FT-IR spectrum of PDVIm-Fe/PDA after use.
Figure S15. UV-vis spectra of MO under different conditions.
Figure S16. The HPLC chromatograms of CIP during the different degradation time intervals.
Figure S17. Chemical structure of CIP and its possible byproducts.
Table S4. Comparison of the MG degradation performances with different kinds of catalysts in the literature.

^1H NMR of Free Base DA

Free base DA was dissolved in deuterated methanol (CD_3OD) and analyzed using a Bruker DPX 500 spectrometer. After 32 scans, the proton NMR spectrum was integrated using Maestro NMR analysis software.

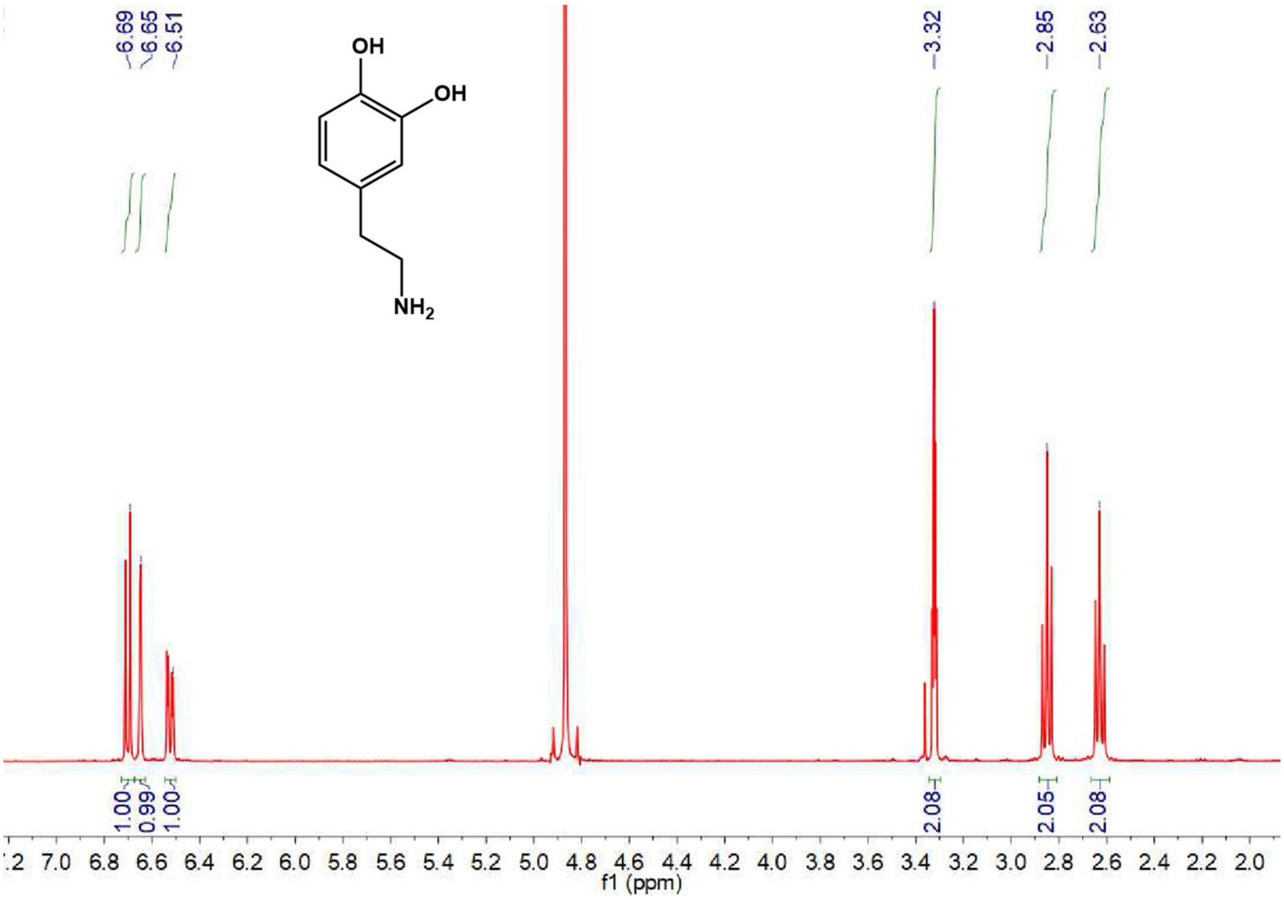

Figure S1. ^1H NMR spectrum of the as-synthesized free base DA.

Scanning Electron Microscopy

Scanning electron microscopy (SEM) analysis was performed on a ZEISS sigma coupled with energy dispersive x-ray (EDX) spectroscopy at an accelerating voltage of 15.0 kV. To minimize electron-charging effects, samples were sputter-coated with platinum (~10 nm thick) in a Quorum-Q150.

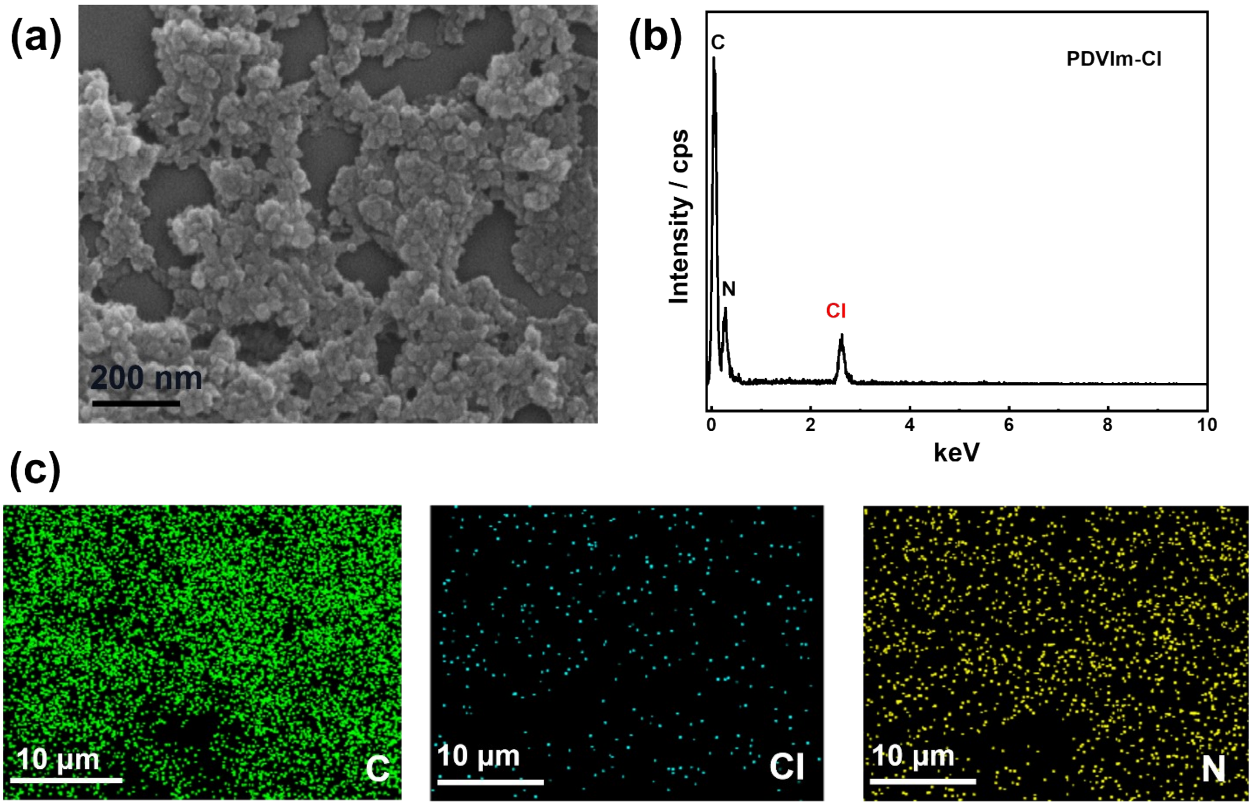

Figure S2. (a) SEM image, (b) EDS spectrum of PDVIm-Cl and (c) the corresponding elemental mappings of C, Cl and N.

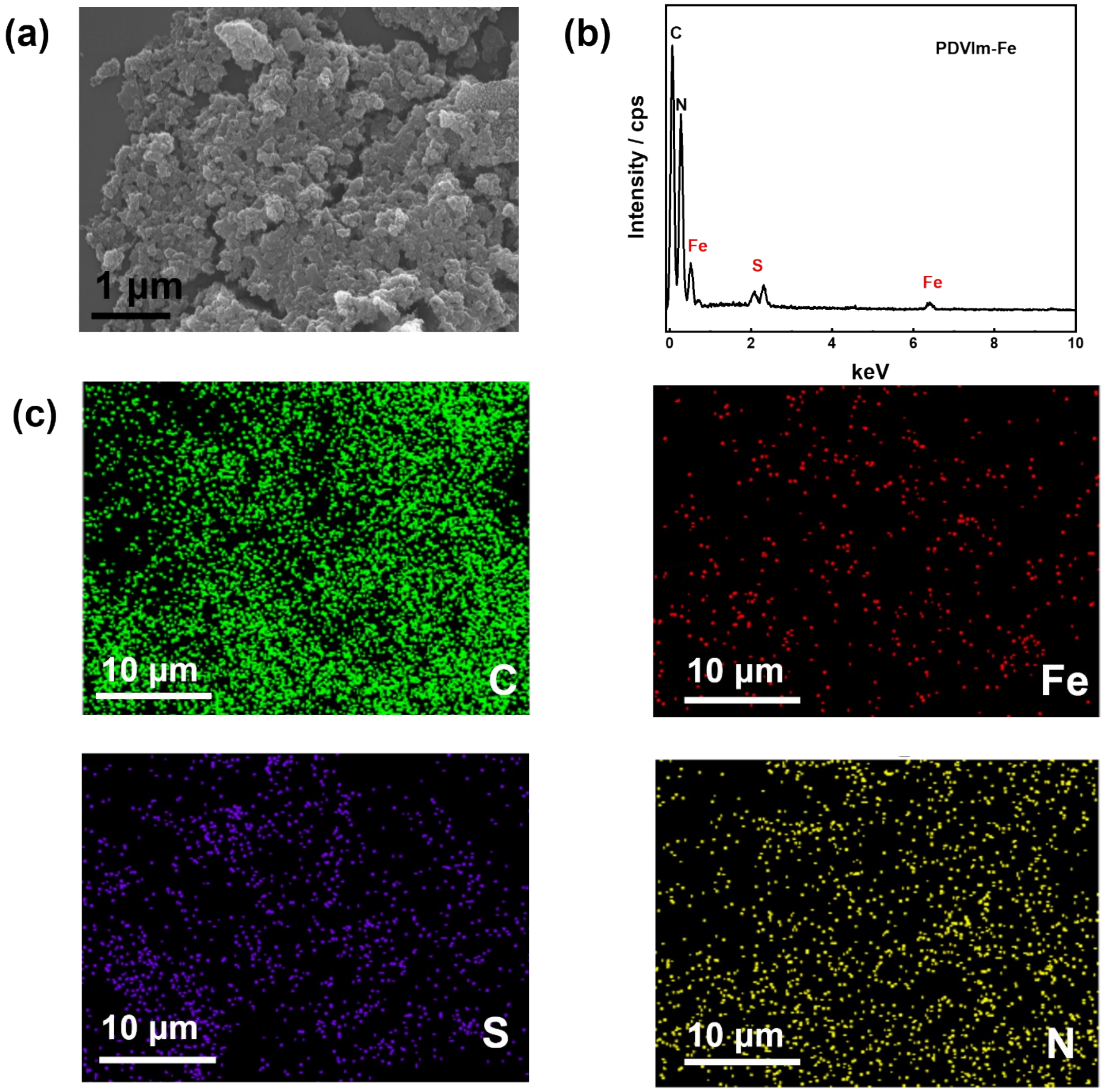

Figure S3. (a) SEM image, (b) EDS spectrum of PDVIm-Fe and (c) the corresponding elemental mappings of C, Fe, S and N.

Element analysis

The Fe contents of PDVIm-Fe, PDVIm-Fe/PDA were determined via ICP-OES and the C H N wt% values were analyzed from the combustion analysis.

Table S1. The element content of PDVIm-Fe, PDVIm-Fe/PDA

Sample	**Weight / mg**	**C/N ratio**	**N%**	**C%**	**S%**	**H%**	**Fe %** [a]
PDVIm-Fe	3.7250	2.293	10.48	23.85	10.09	4.64	13.50
PDVIm-Fe/PDA	3.2880	2.610	10.21	26.64	6.60	4.30	10.50

Nitrogen Adsorption Measurements

100-200 mg PDVIm-Fe or PDVIm-Fe/PDA were transferred to a pre-weighed glass sample tube and degassed under vacuum at 100 °C for 6 h at a ramp rate of 7.0 °C per minute. After cooled to room temperature and back filled with argon, the sample was transferred to a Belsorp-max gas adsorption analyzer and performed at 77 K using liquid N_2.

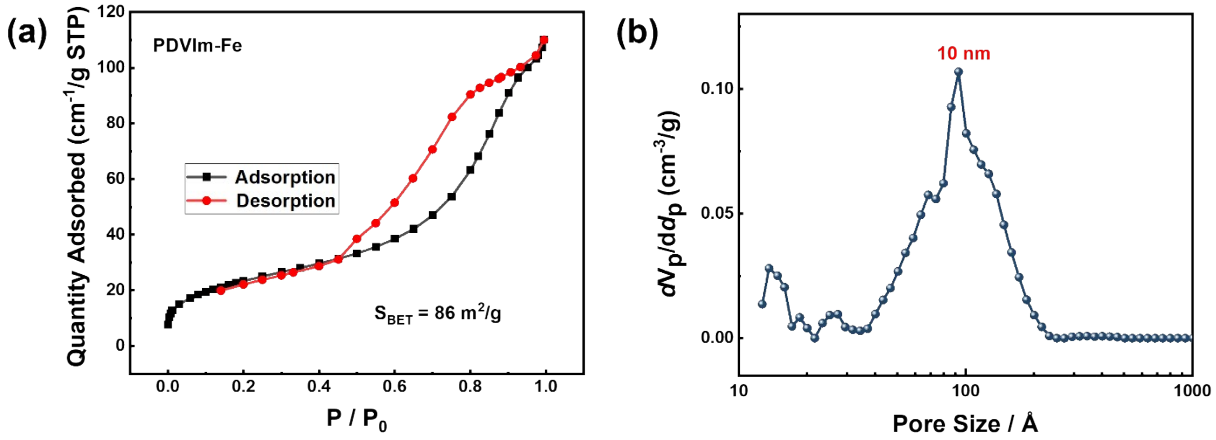

Figure S4. (a) N_2 adsorption and desorption isotherms and (b) pore size distribution curve of PDVIm-Fe.

Fourier Transform Infrared Spectroscopy

The FT-IR spectra of the samples were recorded on a Nicolet 330 infrared spectrometer (Thermo Electron Corporation, USA) in the range from 400 to 4000 cm^{-1} with the resolution of 4 cm^{-1}.

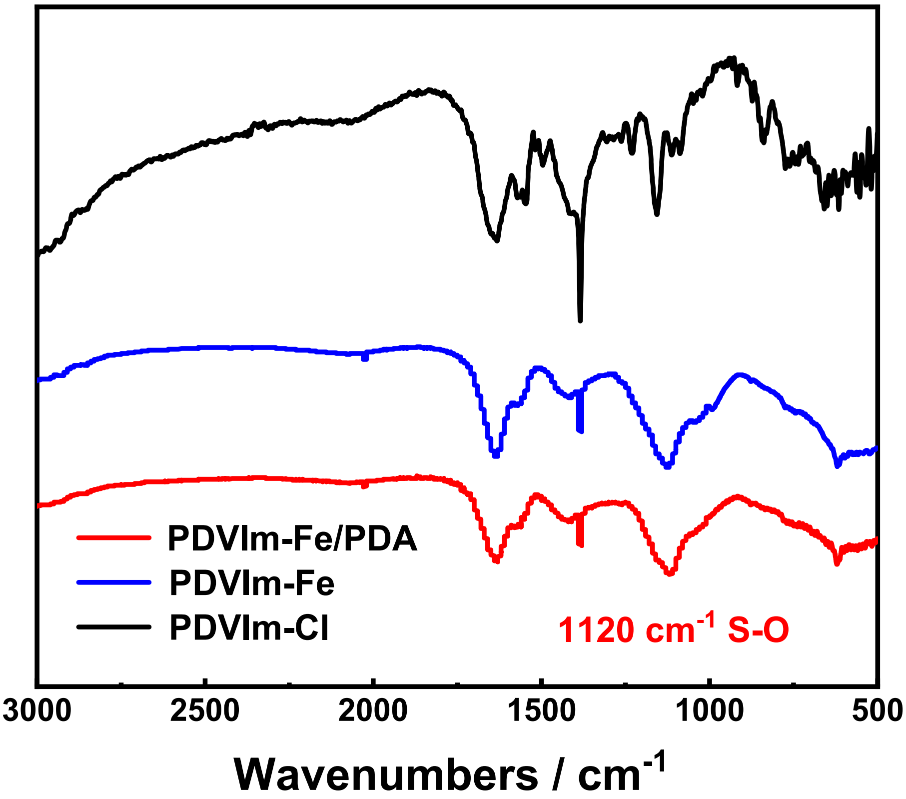

Figure S5. FT-IR spectra of PDVIm-Cl (grey), PDVIm-Fe (blue) and PDVIm-Fe/PDA (red).

Degradation efficiency of PDVIm-Fe/PDA to MG

The UV spectra of MG were measured by a UV-2550 UV-vis spectrophotometer. The absorbance of the peak at 617 nm at different MG concentrations was used as signal to plot the standard curve, as shown in Figure S6.

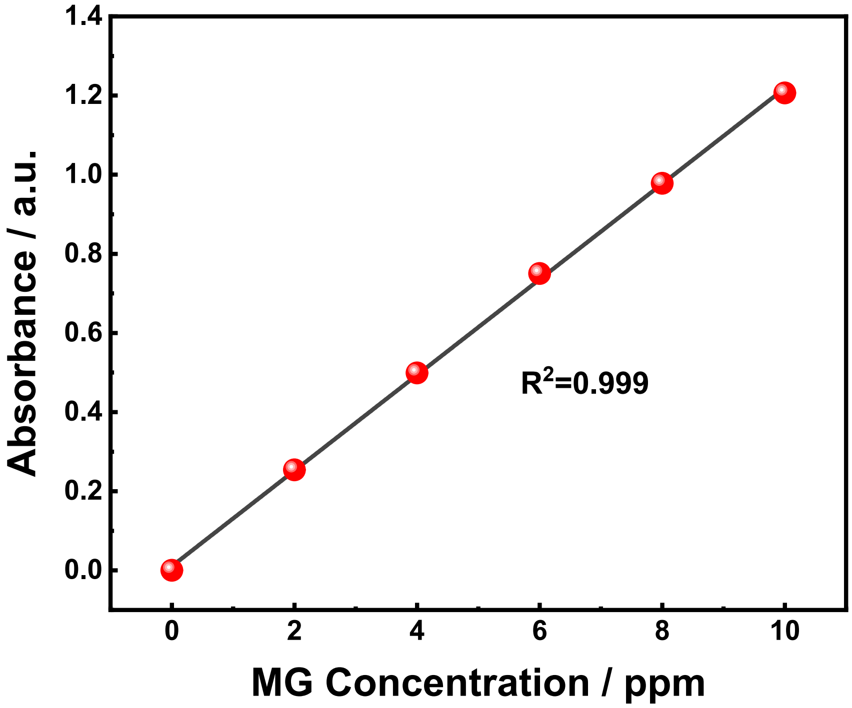

Figure S6. Standard curve of the different concentrations of MG.

The degradation efficiency of MG under different times was calculated with Eq. (S1).

$$D_t = \frac{(C_0 - C_t)}{C_0} \times 100\% \tag{S1}$$

where C_0 (ppm or g L^{-1}) and C_t (ppm or g L^{-1}) are the concentrations of MG at the initial time and t (min). The degradation kinetics data were fitted to Eq. (S2) or Eq.(S3)

$$-\mathrm{d}\, C_t/\mathrm{d}\, t = k\, C_t \tag{S2}$$

$$\ln (C_0/C_t) = kt \tag{S3}$$

where k is the degradation rate constant ($\min^{-1}$).

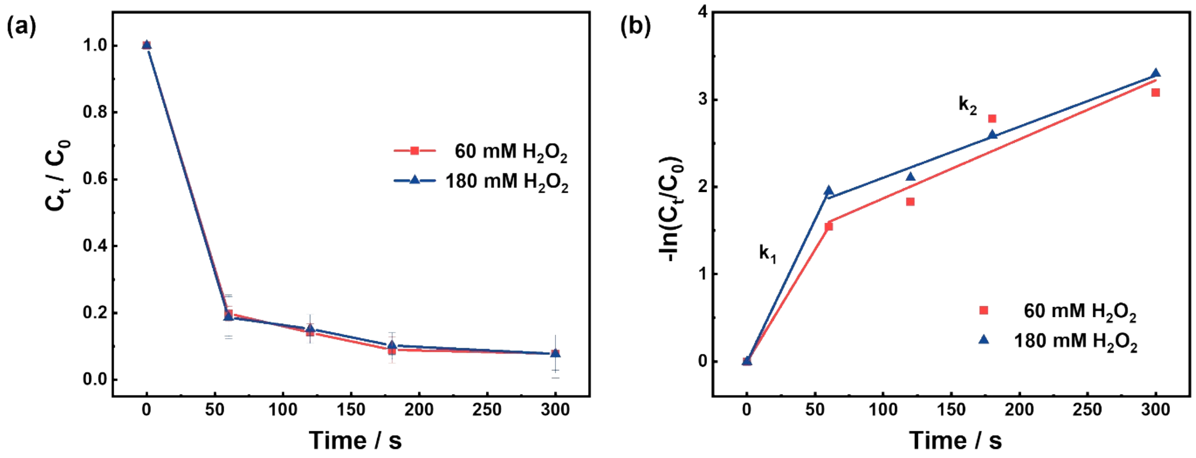

Figure S7. (a) Plots of relative concentration (C_t/C_0) changes of MG and (b) kinetic plots for the degradation of MG under different amounts of H_2O_2. ([catalyst] = 0.25 g/L, [AA] = 6 mM, pH = 7.0).)

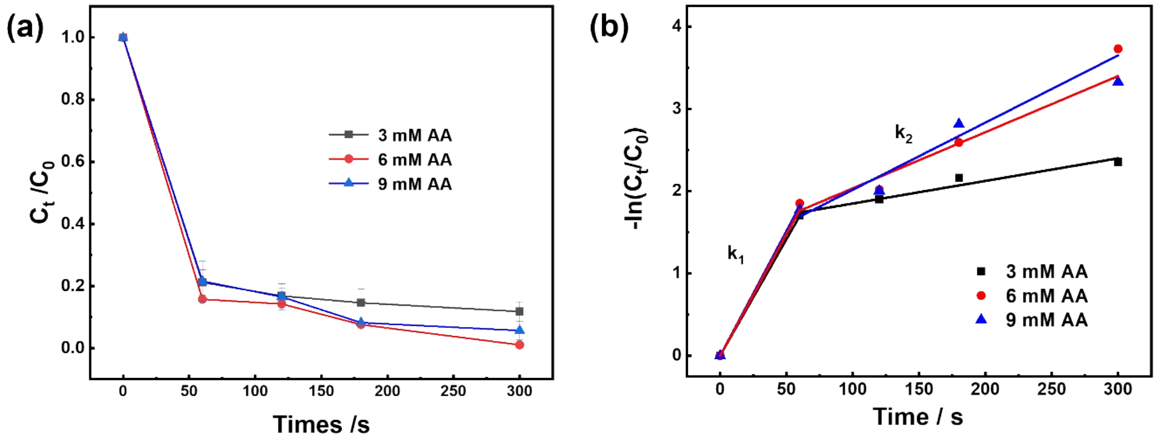

Figure S8. (a) Plots of relative concentration (C_t/C_0) changes of MG and (b) kinetic plots for the degradation of MG under different amounts of AA. ([catalyst] = 0.25 g/L, [H_2O_2] = 120 mM, pH = 7.0)

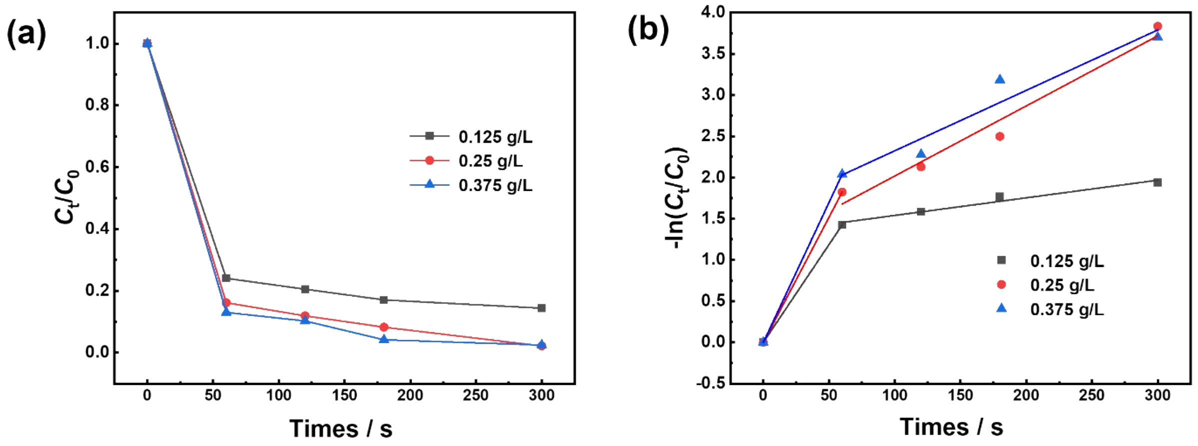

Figure S9. (a) Plots of relative concentration (C_t/C_0) changes of MG and (b) kinetic plots for the degradation of MG under different amounts of catalyst. ([AA] = 6 mM, [H_2O_2] = 120 mM, pH = 7.0)

Table S2. The rate constants of MG degradation by PDVIm-Fe/PDA.

	k_1 (min^{-1})	k_2 (min^{-1})	R_2^2
60 mM H_2O_2	1.54	0.41	0.883
120 mM H_2O_2	1.82	0.49	0.969
180 mM H_2O_2	1.95	0.35	0.981
3 mM AA	1.69	0.17	0.950
9 mM AA	1.77	0.41	0.943
0.125 g/L Catalyst	1.42	0.13	0.967
0.375 g/L Catalyst	2.03	0.44	0.934

Note: k_1 and k_2 are from Eq. (2) or Eq. (3) with different stages (see Fig. 3c and Fig.S7-9b) for k; R_2^2 is the fitting square error for k_2.

Determination of radicals' species and concentration

Quenching experiment was performed by applying different scavengers to determine the contributions of the radicals.

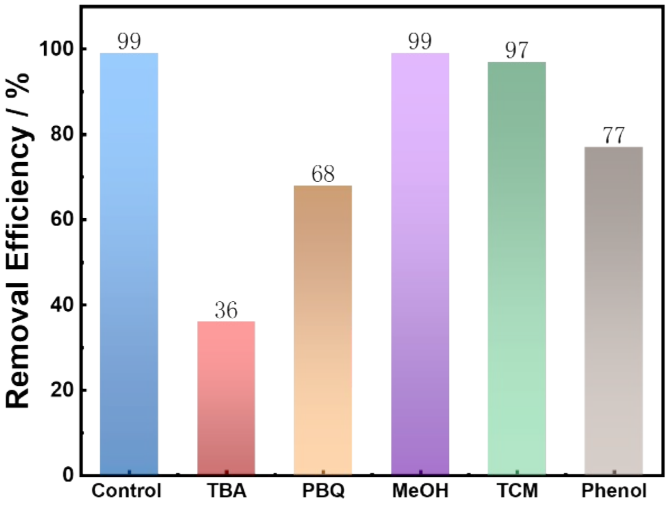

Figure S10. The influence of various quenchers on MG degradation efficiency by PDVIm-Fe/PDA. ([catalyst] = 0.25 g/L, [AA] = 6 mM, [H_2O_2] = 120 mM, pH = 7.0)

2-hydroxy terephthalic acid (product of the reaction of terephthalic acid (PTA) with ·OH radical) and p-hydroxybenzoic acid (p-HBA, react with $SO_4{\cdot}^-$) as fluorescence probe to determine the amount of the radicals produced by PDVIm-Fe/PDA.

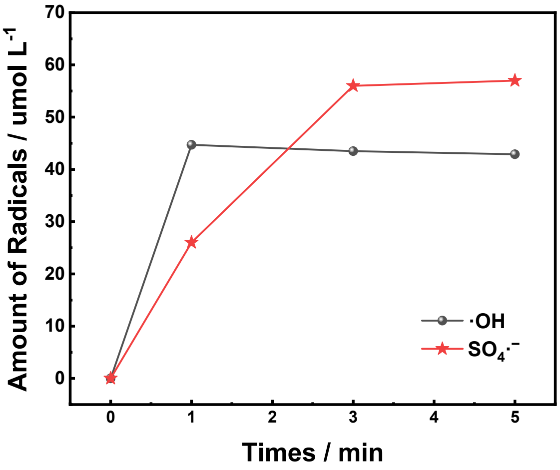

Figure S11. The detected radical concentrations produced by PDVIm-Fe/PDA at different times.

Determination of TOC value

For comparison, 10 mg/L MG, 120 mM H_2O_2 and 3 mM AA were selected as the model reaction conditions to determine the TOC value before and after the reaction. The TOC values were presented in Table S3.

Table S3. The TOC values in the MG degradation process catalyzed by PDVIm-Fe/PDA.

	TOC (mg/L)	TOC/TOC$_0$	TOC removal (%)
MG	4.6 [a]	--	---
AA+ MG (0 min)	202.7 [b]	1	0
1 min	202.4	0.97	2.27
2 min	193.7	0.93	6.47
3 min	183.1	0.88	11.59
4 min	181.1	0.87	12.60
5 min	181.4	0.87	12.60

[a] Theoretically, TOC_{MG0} = 10 ×75% ×97% = 7.2 mg/L

[b] Theoretically, $TOC_0 = TOC_{MG0} + TOC_{AA\ 0}$= 7.2 + 3×176×97%×40% = 7.2 + 204.8 = 212.0 mg/L

([MG]=10 mg/L ($C_{MG}\% = M_{C\ in\ MG}/M_{MG}$ = 23×12/365 = 75%, purity = 97%), [catalyst] = 0.25 g/L, [AA] = 3 mM ($C_{AA}\% = M_{C\ in\ AA}/M_{AA}$ = 12×6/176 = 40%, purity = 97%), [H_2O_2] = 120 mM, pH = 7.0)

Stability of PDVIm-Fe/PDA

For comparison, the catalytic efficiency and reusability of PDVIm-Fe and Fe/PDA were also performed within 5 min.

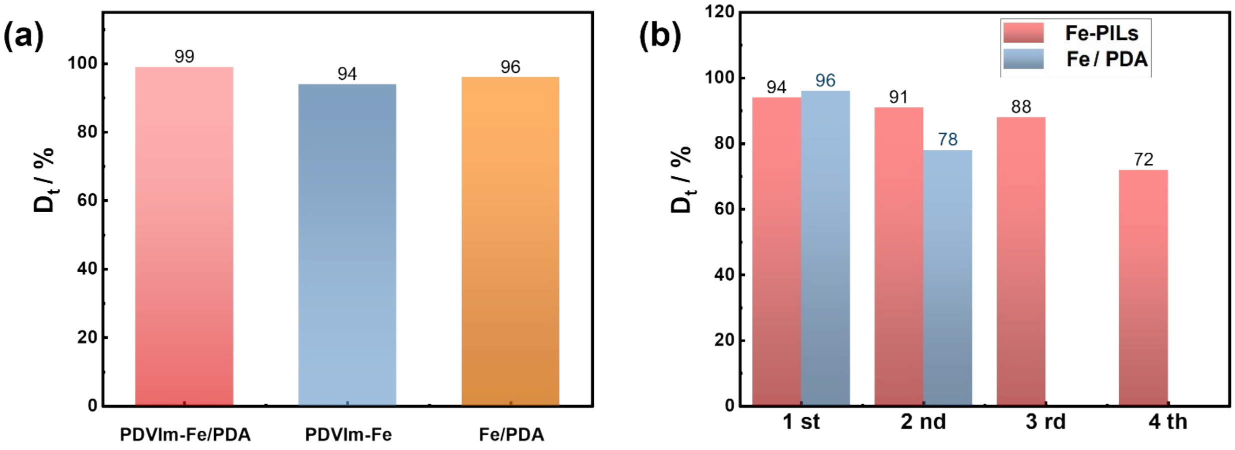

Figure S12. (a) Degradation efficiency of PDVIm-Fe and Fe/PDA on MG and (b) their recyclability. ([catalyst] = 0.25 g/L, [H_2O_2] = 120 mmol/L, [AA] = 6 mmol/L, pH = 7.0)

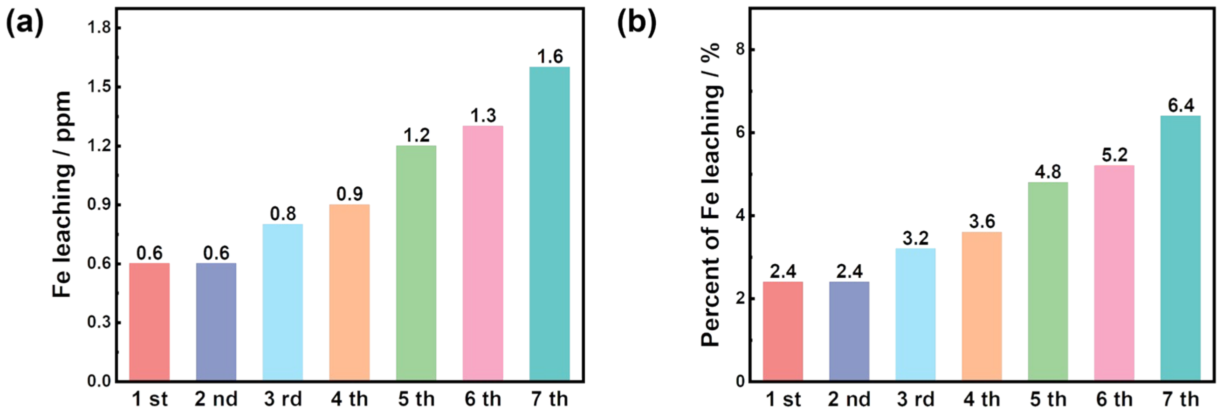

Figure S13. (a) Fe leaching in the solution in each cycling test and (b) percent of Fe leaching in the solution compared with the original iron content in the catalyst. ([catalyst] = 0.25 g/L, [AA] = 6 mM, [H_2O_2] = 120 mM, pH = 7.0)

The chemical structure of PDVIm-Fe/PDA was also analyzed via FT-IR to evaluate its stability.

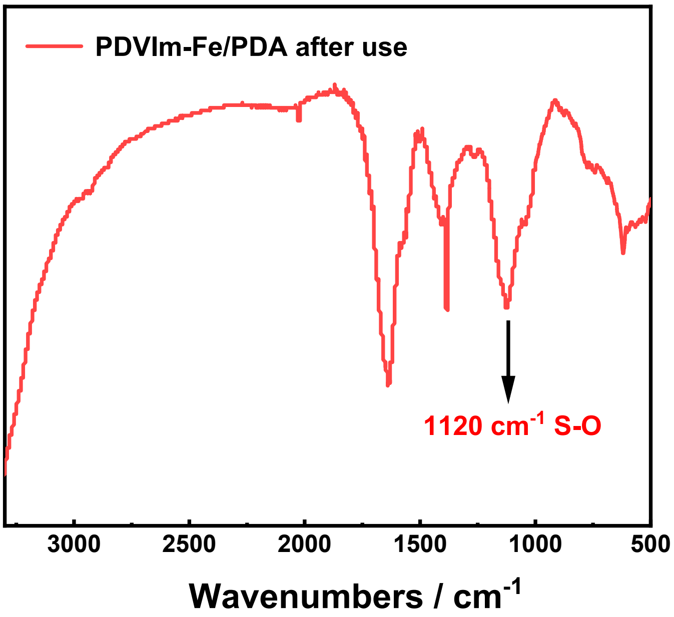

Figure S14. FT-IR spectrum of PDVIm-Fe/PDA after use.

Degradation of anionic dye MO

The adsorption and degradation experiments of PDVIm-Fe/PDA on MO were performed as follows. (1) 5 mg PDVIm-Fe/PDA was added to 50 mL 20 ppm MO solution and allowed to shake in an oscillator for 5 min; (2) After mixing 5 mg PDVIm-Fe/PDA and 50 mL 20 ppm MO, a certain amount of H_2O_2 (30 wt%) and AA was added and then shook for 5 min. After reaction, both the mixtures were filtered through a 0.22 mm membrane and immediately measured via uv-vis spectroscopy.

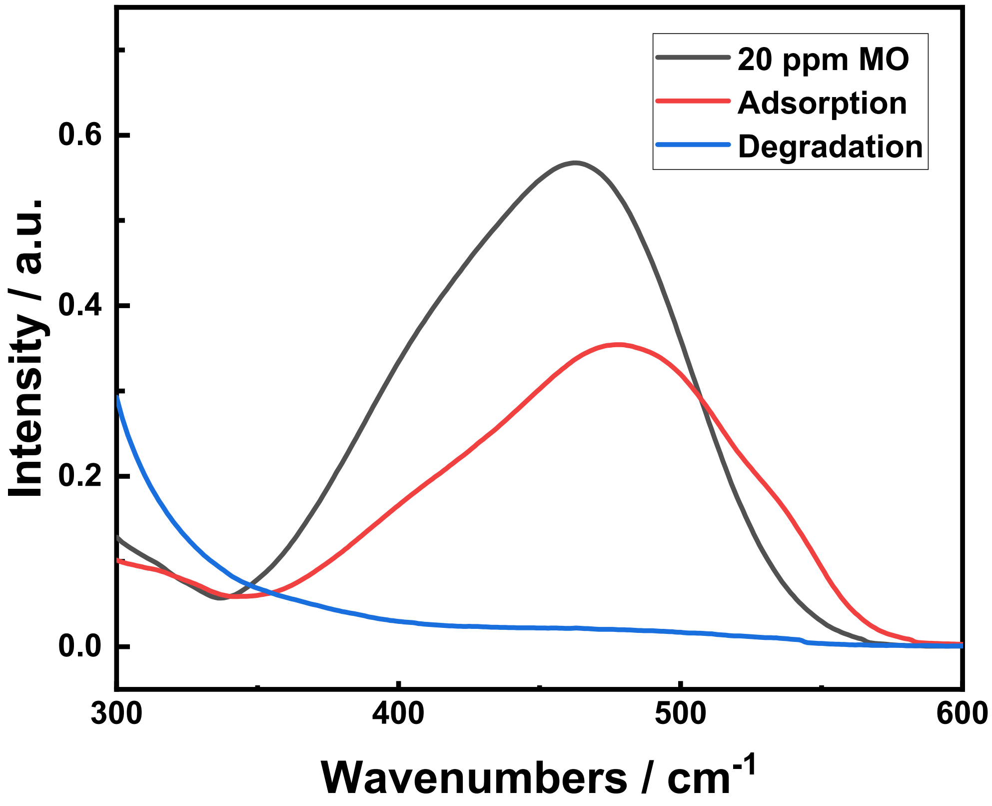

Figure S15. UV-vis spectra of MO under different conditions. ([catalyst] = 0.10 g/L, [H_2O_2] = 240 mM, [AA] = 10 mM)

Degradation of antibiotic CIP

The concentration of CIP was analyzed on high performance liquid chromatography (HPLC, Hitachi, L-2000) equipped with a C18 column. The mobile phase was methanolic aqueous solution containing 0.2% (v/v) formic acid in 30/70 volumetric ratio (V_{MeOH}/V_{H2O}) at a flow rate of 1.0 mL/min.

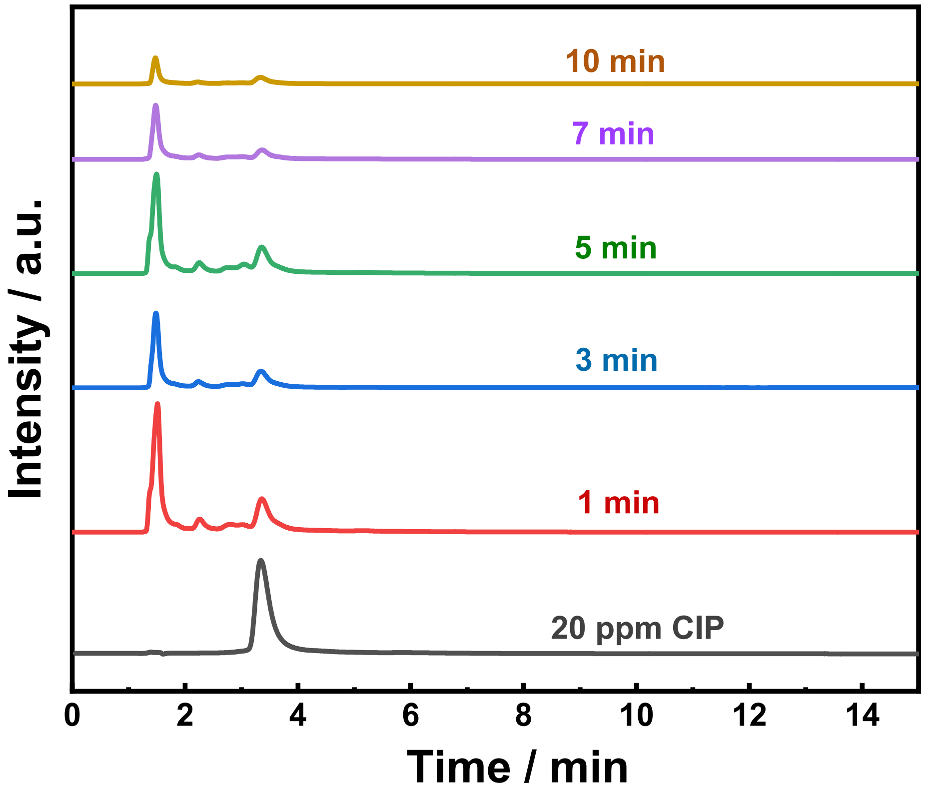

Figure S16. The HPLC chromatograms of CIP during the different degradation time intervals. ([catalyst] = 0.25 g/L, [H_2O_2] = 120 mM, [AA] = 6 mM)

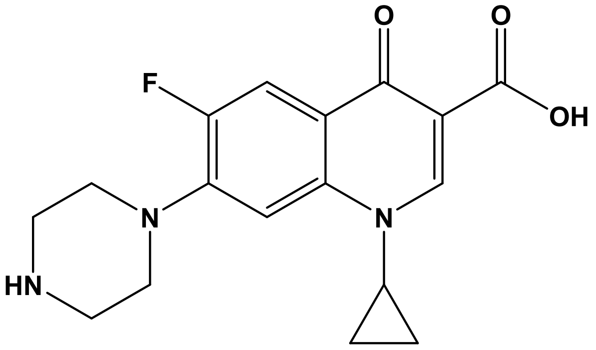

1-cyclopropyl-6-fluoro-4-oxo-7-(piperazin-1-yl)
-1,4-dihydroquinoline-3-carboxylic acid (CIP)

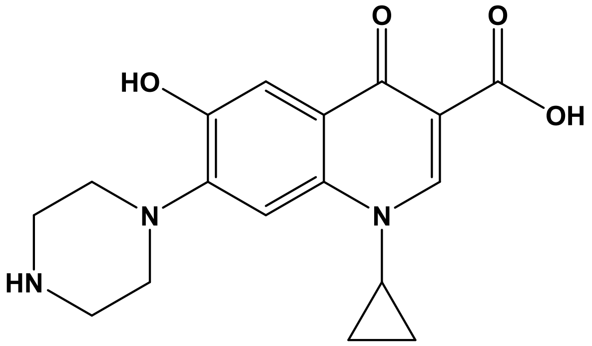

1-cyclopropyl-6-hydroxy-4-oxo-7-(piperazin-1-yl)-
1, 4-dihydroquinoline-3-carboxyl acid

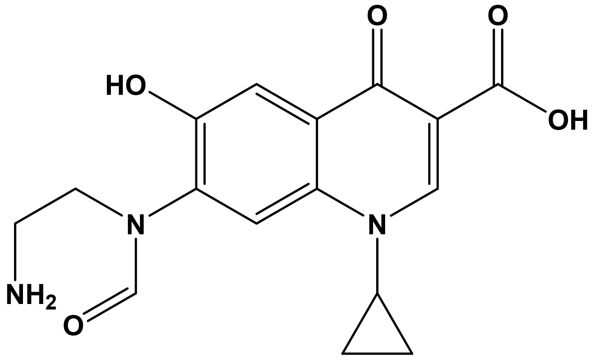

7-[(2-ethylamino) (formyl)amino)-1-cyclopropyl-
4-oxo-1, 4-dihydroquinoline-3-carboxyl acid

Figure S17. Chemical structure of CIP and its possible byproducts.

Comparison of the degradation performances of MG

Table S4. Comparison of the MG degradation performances with different kinds of catalysts in the literature.

Catalyst	m_{cat} /mg	V_{MG} /mL	C_0 /mg L^{-1}	t /min	D_t /%	k /min^{-1}	Cycles	R^a	*Ref.*
PDVIm-Fe/PDA	**10**	**40**	**10**	**5**	**99**	**1.95(k_1)**	**7**	**0.79**	**This work**
Homogenous iron-based catalysts									
$FeSO_4·7H_2O$	6	200	20	60	> 99	--	--	1.1	[1]
$FeSO_4·7H_2O$	200	500	300	--	> 99	--	--	--	[2]
$Fe_2(SO_4)_3·7H_2O$	30	500	9.87	15	95.5	--	--	1.05	[3]
Heterogenous iron-based composites for MG degradation									
$Zn/HAP/MgFe_2O_4$	40	70	10	2	99	4.01	7	0.87	[4]
Fe/FBC	50	200	10	5	98	0.05	10	0.78	[5]
Fe_3O_4/graphene aerogels	10	50	20	12	99	0.21	6	0.83	[6]
$CuFe_2O_4$@BC	20	100	100	80	99	--	5	0.62	[7]
Fe-N-C/CNx	10	50	80	140	92	0.011	4 (86% in 2nd)	0.26	[8]
$Fe-TiO_2$/AC	100	100	100	60	97	--	--	0.16	[9]
Core-Shell $Fe_3O_4@SiO_2$	15	25	25	30	94	0.11	4 (70% in 2nd)	0.13	[10]
Fe_3O_4@SBA-15	35	100	15	60	99	0.19	5	0.07	[11]

Fe-CF	1000	1000	36	120	99	--	6	0.03	12
Fe0-BG	60	50	13	60	99	0.08	6 (75 % in 6th)	0.02	13
Fe@(Alg-CMC)	100	50	10	30	99	0.12	--	0.02	14
Other heterogeneous composites for MG degradation									
cl-Ch-pMAc @ZnO/CdSQDs	10	50	100	300	98	0.012	5	0.87	15
$Fe_{0.01}Ni_{0.01}Zn_{0.98}O$/polyacrylamide nanocomposite	25	100	4	240	97	0.034	5	0.83	16
GO-ZnO/Mn_2O_3	20	100	50	40	99	0.14	5	0.78	17
rGO/ZnO	25	50	4	140	99	0.025	-	0.16	18
CuO/$PbTiO_3$	20	20	100	180	91	0.017	6	0.13	19
ZnO/CNT	10	100	30	60	79	--	4	0.02	20
diatomite/$MnSiO_3$	30	100	500	70	93	0.06	5	0.01	21
PANI/ZnO	0.25	2.5	4	300	99	0.024	5	0.01	222

[a] Besides the degradation efficiency D_t, degradation rate constant k, a universal catalytic degradation rate R in g(degraded matter) g(catalyst)$^{-1}$ min^{-1}, similar to the common product evolution rate for evaluating a catalyst performance, was proposed and defined (Eq.S4) for reasonable comparison of the catalytic performance of all the systems in the table.

$$R = (C_0 - C_f)V_{MG}/m_{cat}/t_f = C_0 D_t V_{MG}/\ m_{cat}/t_f \qquad \text{(S4)}$$

where C_f (mg L^{-1}) is the C_t at the time t_f when the degradation efficiency reaches the final D_t listed in the table ($D_t \geq 99\%$ is normally necessary), V_{MG} is the volume of the MG solution applied for degradation, m_{cat} is the mass of the catalyst.

References

1. B. H. Hameed and T. W. Lee, Degradation of malachite green in aqueous solution by Fenton process, *J. Hazard. Mater.*, 2009, **164**, 468-472.
2. S. Thakur, and M. S. Chauhan, Removal of malachite green dye from aqueous solution by Fenton oxidation, *Int. Res. J. Eng. Technol*. 2016, **3**, 254-259.
3. S. Hashemian, Fenton-like oxidation of malachite green solutions: kinetic and thermodynamic study, *J. Chem.*, 2013, **2013**, 1-7.
4. K. C. Das and S. S. Dhar, Remarkable catalytic degradation of malachite green by zinc supported on hydroxyapatite encapsulated magnesium ferrite (Zn/HAP/$MgFe_2O_4$) magnetic novel nanocomposite, *J. Mater. Sci.*, 2019, **55**, 4592-4606.
5. L. He, S.-S. Yang, S.-W. Bai, J.-W. Pang, G.-S. Liu, G.-L. Cao, L. Zhao, X.-C. Feng and N.-Q. Ren, Fabrication and environmental assessment of photo-assisted Fenton-like Fe/FBC catalyst utilizing mealworm frass waste, *J. Clean. Prod.*, 2020, **256**, 120259.
6. J. Lu, Y. Zhou, J. Lei, Z. Ao and Y. Zhou, Fe_3O_4/graphene aerogels: a stable and efficient persulfate activator for the rapid degradation of malachite green, *Chemosphere*, 2020, **251**, 126402.
7. Q. Huang, C. Chen, X. Zhao, X. Bu, X. Liao, H. Fan, W. Gao, H. Hu, Y. Zhang and Z. Huang, Malachite green degradation by persulfate activation with $CuFe_2O_4$@biochar composite: Efficiency, stability and mechanism, *J. Environ. Chem. Eng.*, 2021, **9**.
8. S. Huang, B. Hu, S. Zhao, S. Zhang, M. Wang, Q. Jia, L. He, Z. Zhang and M. Du, Multiple catalytic sites of Fe-N and Fe-N-C single atoms embedded N-doped carbon heterostructures for high-efficiency removal of malachite green, *Chem. Eng. J.*, 2022, **430**, 132993.
9. W. W. Loo, Y. L. Pang, S. Lim, K. H. Wong, C. W. Lai and A. Z. Abdullah, Enhancement of photocatalytic degradation of Malachite Green using iron doped titanium dioxide loaded on oil palm empty fruit bunch-derived activated carbon, *Chemosphere*, 2021, **272**, 129588.
10. N. Mahmud, A. Benamor, M. S. Nasser, M. M. Ba-Abbad, M. H. El-Naas and A. W. Mohammad, Effective heterogeneous Fenton-like degradation of malachite green dye using the core-shell Fe_3O_4@SiO_2 Nano-Catalyst, *ChemistrySelect.*, 2021, **6**, 865-875.
11. H. Aliyan, R. Fazaeli and R. Jalilian, Fe_3O_4@mesoporous SBA-15: A magnetically recoverable catalyst for photodegradation of malachite green, *Appl. Surf. Sci.*, 2013, **276**, 147-153.
12. X. Liu, R. Tang, Q. He, X. Liao and B. Shi, Fe(III)-loaded collagen fiber as a heterogeneous catalyst for the photo-assisted decomposition of malachite green, *J. Hazard. Mater.*, 2010, **174**, 687-693.
13. P. Raizada, P. Singh, A. Kumar, B. Pare and S. B. Jonnalagadda, Zero valent iron-brick grain nanocomposite for enhanced solar-Fenton removal of malachite green, *Sep. Purif. Technol.*, 2014, **133**, 429-437.
14. D. Karadeniz, N. Kahya and F. B. Erim, Effective photocatalytic degradation of malachite green dye by Fe(III)-cross-linked alginate-carboxymethyl cellulose composites, *J. Photochem. Photobiol. A,* 2022, **428**, 113867.
15. L. Midya, A. S. Patra, C. Banerjee, A. B. Panda and S. Pal, Novel nanocomposite derived from ZnO/CdS QDs embedded crosslinked chitosan: An efficient photocatalyst and effective antibacterial agent, *J. Hazard. Mater.*, 2019, **369**, 398-407.
16. S. Kant, D. Pathania, P. Singh, P. Dhiman and A. Kumar, Removal of malachite green and methylene blue by Fe0.01Ni0.01Zn0.98O/polyacrylamide nanocomposite using coupled adsorption and photocatalysis, *Appl. Catal. B*, 2014, **147**, 340-352.
17. D. R. Rout, S. Chaurasia and H. M. Jena, Enhanced photocatalytic degradation of malachite green using

manganese oxide doped graphene oxide/zinc oxide (GO-ZnO/Mn2O3) ternary composite under sunlight irradiation, *J Environ Manage*, 2022, **318**, 115449.

18. H. Y. He, J. Fei and J. Lu, High photocatalytic and photo-Fenton-like activities of ZnO–reduced graphene oxide nanocomposites in the degradation of malachite green in water, *Micro & Nano Letters*, 2015, **10**, 389-394.
19. K. H. Reddy, K. Parida and P. K. Satapathy, CuO/PbTiO3: A new-fangled p–n junction designed for the efficient absorption of visible light with augmented interfacial charge transfer, photoelectrochemical and photocatalytic activities, *Journal of Materials Chemistry A*, 2017, **5**, 20359-20373.
20. N. Arsalani, S. Bazazi, M. Abuali and S. Jodeyri, A new method for preparing ZnO/CNT nanocomposites with enhanced photocatalytic degradation of malachite green under visible light, *Journal of Photochemistry and Photobiology A: Chemistry*, 2020, **389**.
21. D. B. Jiang, Y. Yuan, D. Zhao, K. Tao, X. Xu and Y. X. Zhang, Facile synthesis of three-dimensional diatomite/manganese silicate nanosheet composites for enhanced Fenton-like catalytic degradation of malachite green dye, *Journal of Nanoparticle Research*, 2018, **20**.
22. V. Eskizeybek, F. Sarı, H. Gülce, A. Gülce and A. Avcı, Preparation of the new polyaniline/ZnO nanocomposite and its photocatalytic activity for degradation of methylene blue and malachite green dyes under UV and natural sun lights irradiations, *Applied Catalysis B: Environmental*, 2012, **119-120**, 197-206.